### Title
Phenotypic and Morphological Properties of Germinal Center Dark Zone Cxcl12-Expressing Reticular Cells.




### Journal
Journal of Immunology, 195(10)



### Authors
Rodda, Lauren
Bannard, Oliver
Ludewig, Burkhard
et al.



### Publication Date
2015-11-15

### DOI
10.4049/jimmunol.1501191

Peer reviewed

HHS Public Access

Author manuscript

*J Immunol*. Author manuscript; available in PMC 2016 May 15.

Published in final edited form as:

*J Immunol*. 2015 November 15; 195(10): 4781–4791. doi:10.4049/jimmunol.1501191.

# Phenotypic and morphological properties of germinal center dark zone *Cxcl12*-expressing reticular cells (CRCs) [1,,2]

**Lauren B. Rodda**[*], **Oliver Bannard**[*,1], **Burkhard Ludewig**[†], **Takashi Nagasawa**[‡,x], and **Jason G. Cyster**[*]

[*]Howard Hughes Medical Institute, Department of Microbiology and Immunology, University of California, San Francisco, San Francisco, CA 94143 [†]Institute of Immu- nobiology, Kantonsspital St. Gallen, 9007 St. Gallen, Switzerland [‡]Department of Immunobiology and Hematology, Institute for Frontier Medical Sciences, Kyoto Uni- versity, Kyoto 606-8507, Japan [x]Japan Science and Technology Agency, Core Research for Evolutional Science and Technology, Kyoto 606-8507, Japan

## Abstract

The germinal center (GC) is divided into a dark zone (DZ) and a light zone (LZ). GC B cells must cycle between these zones to achieve efficient antibody affinity maturation. Follicular dendritic cells (FDCs) are well characterized for their role in supporting B cell antigen encounter in primary follicles and in the GC LZ. However, the properties of stromal cells supporting B cells in the DZ are relatively unexplored. Recent work identified a novel stromal population of *Cxcl12*-expressing reticular cells (CRCs) in murine GC DZs. Here we report that CRCs have diverse morphologies, appearing in 'open' and 'closed' networks, with variable distribution in lymphoid tissue GCs. CRCs are also present in splenic and peripheral lymph node primary follicles. Real-time two-photon microscopy of Peyer's patch GCs demonstrates B cells moving in close association with CRC processes. CRCs are gp38$^{+}$ with low to undetectable expression of FDC markers, but CRC-like cells in the DZ are lineage marked, along with FDCs and FRCs, by *CD21*-Cre and *Ccl19*-Cre directed fluorescent reporters. In contrast to FDCs, CRCs do not demonstrate dependence on lymphotoxin or TNF for chemokine expression or network morphology. CRC distribution in the DZ does require CXCR4 signaling, which is necessary for GC B cells to access the DZ and likely to interact with CRC processes. Our findings establish CRCs as a major stromal cell type in the GC DZ and suggest CRCs support critical activities of GC B cells in the DZ niche through *Cxcl12* expression and direct cell-cell interactions.

[1]This work and L.B.R were supported by National Institutes of Health Grant AI45073. O.B. is supported by a Sir Henry Dale Fellowship of the Wellcome Trust/Royal Society. J.G.C. is an investigator of the Howard Hughes Medical Institute.

[2]Abbreviations: CRC, *Cxcl12*-expressing reticular cell; DZ, dark zone; FDC, follicular dendritic cell; FRC, fibroblastic reticular cell; GC, germinal center; LN, lymph node; LT, lymphotoxin; LZ, light zone; TNF, tumor necrosis factor

[‡]Address correspondence and reprint requests to Dr. Jason G. Cyster, University of California San Francisco, 513 Parnassus Avenue, Box 0414, HSE 1001, San Francisco, CA 94143. Phone: 415-502-6427, Fax: 415-502-8424, Jason.Cyster@ucsf.edu.

[1]Current address: MRC Human Immunology Unit, Weatherall Institute of Molecular Medicine, University of Oxford, Oxford, U.K.

## INTRODUCTION

Lymphoid tissue stromal cells are specialized mesenchymal cells that establish and maintain the distinct niches necessary to support effective adaptive immune responses. Lymphoid follicles, the B cell rich regions of lymphoid organs, are organized around a complex network of follicular stromal cells (1). Many of the follicular stromal cells in primary (non-reactive) follicles produce the chemokine CXCL13 (BLC) and are involved in attracting B cells into this compartment. Follicular dendritic cells (FDCs) are a subset of these CXCL13-expressing stromal cells situated in the central region of the follicle (1). First defined by their ability to capture opsonized antigens, FDCs are now known to highly express complement receptors-1 and -2 (CD35 and CD21 respectively) and Fcγ receptors to support the process of immune complex capture and display to cognate B cells (1–3). FDCs and the broader CXCL13-producing follicular stromal cell network share a dependence on the cytokines lymphotoxin-α1β2 (LT) and TNF for maintenance and function (4–6).

While FDCs are one of the stromal cell types supporting B cell follicles, fibroblastic reticular cells (FRCs) are mesenchymal stromal cells that support the structure and function of the T zone. FRCs produce the chemokines CCL19 and CCL21 in a LT-dependent manner to guide CCR7-expressing B and T cells into lymph node (LN) and splenic T zones (4, 7, 8). FRCs also promote T cell homeostasis by producing IL-7 (9). Additionally, FRCs form a network of conduits in the T zone that transport antigen and facilitate T cell encounter with antigen-bearing dendritic cells (10).

Following antigen exposure, activated B cells proliferate in B cell follicles and form polarized germinal centers (GCs), each with a light zone (LZ) and a dark zone (DZ). The FDCs within GCs upregulate CD21, CD35, Fc receptors, ICAM1 and VCAM1 and show increased staining for activated complement 4 (C4, FDC-M2) and milk fat globule epidermal growth factor 8 (MFG-E8, FDC-M1) relative to FDCs in primary follicles (2). Antigen-bearing FDCs are restricted to the LZ designating this as the site of B cell antigen recognition and selection (11). GC FDCs have also been shown to be essential for GC B cell confinement and viability (12). CXCL13 is present in the GC LZ and plays a role in positioning GC B cells in this region. In contrast, the DZ has little CXCL13 and instead is a source of CXCL12 (SDF1). GC B cell movement from LZ to DZ as well as GC polarization into zones depends on GC B cell expression of the CXCL12 receptor CXCR4 (13). Once in the DZ, GC B cells express higher amounts of activation-induced cytidine deaminase, undergo somatic hypermutation and are more likely to proliferate before returning to the LZ (1, 14). Recent work has highlighted the importance of the DZ for affinity maturation and GC participation as these were impaired in CXCR4 knockout GC B cells that could not access the DZ (15).

In contrast to the extensive study of FDCs since their discovery in the 1960’s, little is known about the stromal cells in the GC DZ. Ultrastructural studies revealed the presence of stromal cells in the DZ of human tonsil GCs and referred to them as immature FDCs even though they mostly did not capture or display opsonized antigen, lacked the ‘labyrinth-like’ structure of LZ FDCs and their relationship to true antigen-capturing FDCs was unclear (16, 17). Lefevre and coworkers described a mAb, found to bind fibrinogen, that stained DZ

stromal cells in bovine and ovine GCs (18). However, fibrinogen was found not to be made locally by the DZ stroma and was thought to have derived from blood or lymph. In recent work, we followed up on the functional evidence that CXCL12 emanates from the DZ (13) to reveal the existence of *Cxcl12*-expressing reticular cells (CRCs) in mediastinal LN GC DZs after influenza (15). While CRCs have only minimal overlap with reticular fibers in the mediastinal LN, CRCs were so named to represent their net-like morphology, as the term 'reticular' comes from the latin word for 'net' (1). This work also provided initial evidence that related cells were present in Peyer's patches (PPs) and within peripheral LN (pLN) primary follicles. However, whether CRCs are a homogeneous population across tissues, what lineage relationships they have to surrounding stroma and what distinguishing requirements they have for maturation and maintenance were not established.

Here we demonstrate that CRC networks have two distinct morphologies and are present in the GC DZs of spleens and pLNs after viral infection. We also find CRCs within the chronic GCs of mesenteric LNs (MLNs) as well as PPs. GC B cells migrate over CRC processes in a similar manner to their migration over FDC processes. While CRCs are phenotypically distinguishable from FDCs and FRCs, they are likely related in origin based on lineage tracing experiments using *CD21*-Cre and *Ccl19*-Cre transgenic mice. Distinct from FDCs, CRCs do not require LT or TNF for short-term maintenance of chemokine expression or morphology. Organization of CRCs into reticular networks, however, depends on CXCR4 function.

## MATERIALS AND METHODS

### Mice and chimeras

C57BL/6 (B6) and B6-CD45.1 mice were obtained from The Jackson Laboratory or the National Cancer Institute. *B6.Cg-Cxcl12*$^{tm2Tng}$ (*Cxcl12*-GFP) gene-targeted mice were backcrossed to the C57BL/6 background more than 7 generations and provided by T. Nagasawa (19). *Tg(UBC-GFP)30Scha/J* (UBI-GFP) transgenic mice were backcrossed to the C57BL/6 background for more than 8 generations and were from The Jackson Laboratory (20). *B6.Tg(Cr2-Cre)3Cgn* (*CD21*-Cre) BAC-transgenic mice were fully backcrossed to C57BL/6 and provided by K. Rajewsky (Immune Disease Institute, Boston, MA) (21). *B6.Cg-Gt(ROSA)26Sor*$^{tm6(CAG-Zsgreen1)Hze/J}$ (*R26*-ZsGreen) mice have a CAG promoter, a floxed stop sequence and ZsGreen1 knocked into the Gt(ROSA)26Sor locus and were from The Jackson Laboratory. *C57BL/6N-Tg(Ccl19-cre)*$^{489Biat}$ (*Ccl19*-Cre) BAC-transgenic mice (8) were provided by C. Lowell. *Gt(ROSA)26Sor*$^{tm1(EYFP)Cos}$ (*R26*-EYFP) transgenic mice express EYFP from the Gt(ROSA)26Sor locus after Cre-mediated deletion of floxed stop cassette (22) and were provided by L. Lanier. *Tg(CAG-ECFP)CK6Nagy* (CFP) transgenic mice were backcrossed to the C57BL/6 background more than 5 generations and were from The Jackson Laboratory. *Tg(IghelMD4)4Ccg* (MD4) transgenic mice were fully backcrossed to C57BL/6 and were from an internal colony.

To make bone marrow (BM) chimeras, UBI-GFP mice were treated intraperitoneally (i.p.) with 500μg anti-Thy1.2 (clone 30H12) before being lethally irradiated and reconstituted for at least 8 weeks with wild-type CD45.1 BM. *CD21*-Cre mice were crossed to *R26*-ZsGreen

mice and lethally irradiated and reconstituted for at least 8 weeks with wild-type CD45.1 BM as described previously (15).

Animals were housed in a specific pathogen–free environment in the Laboratory Animal Research Center at the University of California, San Francisco (UCSF), and all experiments conformed to ethical principles and guidelines approved by the UCSF Institutional Animal Care and Use Committee.

### Infections and Immunizations

Mice were infected with acute LCMV-Armstrong intravenously (i.v.) at $2.5x10^5$ pfu and analyzed at day 15 for GCs in pLN and spleen (23). For induction of spleen GCs, mice were immunized i.p. with $2x10^8$ SRBCs (Colorado Serum Company) on day 0 and day 5 and were analyzed on day 10–12. For induction of pLN GCs, animals were immunized subcutaneously (s.c.) at the shoulders, flanks and above the tail with SRBCs on day 0 and day 5. Draining pLNs (axillary, brachial and inguinal) were analyzed on day 10–12.

### Treatments and Transfers

For LTβR and TNFR signaling blockade, *Cxcl12*-GFP mice were immunized i.p. or s.c. with SRBCs on day 0 and day 5 and on day 10 treated i.v. with 100μl each of 1mg/ml mLTβR-huIgG1 (LTβR-Fc, provided by J. Browning) and 1mg/ml TNFR55-huIgG1 (TNFR-Fc, provided by J. Browning) or saline. Tissues were analyzed 4 days later.

For CXCR4 inhibitor treatment, *Cxcl12*-GFP mice were immunized with SRBC i.p. on day 0 and day 5. On day 8, Alzet osmotic pumps (1-day duration, 8.4μl/h pumping rate; Model 2001D; Durect Corporation) loaded with saline or 5mg/ml of the CXCR4 antagonist 4F-benzoyl-TE14011 (24) in saline were implanted dorsally s.c. according to the manufacturer's instructions. As analgesics, Buprenorphine (0.05–0.1 mg/kg, Sigma-Aldrich) was given i.p. before and after surgery, Carprofen (5mg/kg, Pfizer Animal Health) was given i.p. before surgery and Bupivicaine (100μl of 0.25%, Hospira, Inc.) was given topically during surgery. Tissues were analyzed 12 or 24 hours later.

For two-photon laser scanning microscopy (TPLSM) of intact GCs from pLNs and MLNs, *Cxcl12*-GFP mice were immunized with SRBC s.c. on day 0 and day 5. On day 8, mice were injected with 2 mg rabbit IgG anti-PE (200-4199, Rockland) i.p. and 12 hours later injected with 75 μg PE (P-801, Invitrogen Molecular Probes) s.c. as previously described (25, 26). On day 9, mice were transferred $1.5 \times 10^8$ CFP transgenic B cells purified from donor spleens using anti-CD43 microbeads (Miltenyi Biotec) i.v. as previously described (26). PLNs and MLNs were mounted and imaged 24 hours later.

For TPLSM of PPs, *Cxcl12*-GFP mice were crossed to MD4 mice and transferred with 20% CFP transgenic B cells and 80% CD45.1 WT B cells. B cells were purified from donor spleens as above and $1.2 \times 10^7$ total B cells were injected i.v. into *Cxcl12*-GFP MD4 mice. Two weeks later the mice were injected i.v. with $2 \times 10^7$ purified CD45.1 WT B cells labeled with CellTracker orange 5-(and-6)-(((4-chloromethyl)benzoyl)amino)tetramethylrhodamine (CMTMR, C2927, Invitrogen) as previously described (26). Experiment was repeated as above with transfer of 5% CFP

transgenic B cells for 4 weeks and 10% CFP transgenic B cells for 2 weeks with similar results. PPs were mounted and imaged 24 hours later.

## Confocal Microscopy

Confocal microscopy was preformed as described previously with some modifications (15). Tissues were fixed in 4% PFA in PBS for 2 hours at 4°C, washed 3 times for 10 min in PBS, then moved to 30% sucrose in PBS overnight. Tissues were flash frozen in TAK tissue-mounting media the following day, and 30μM sections were cut and then dried for 1 hour prior to staining. Sections were rehydrated in PBS with 1% BSA for 10 min and then blocked for 1 hour at room temperature, stained in primary antibody overnight at 4°C and stained for subsequent steps for 2 hours at room temperature all in PBS with 2% mouse serum, 0.1% BSA, 0.3% Triton X-100 and 0.1% NaN3.

For gp38 staining, LNs were fixed in 4% PFA in PBS overnight at 4°C, washed 3 times in PBS, then moved to 20% sucrose in PBS overnight. Sections were processed as above except for rinse in PBS and peroxidase quench in PBS with 0.045% $H_2O_2$ for 15 min prior to blocking for 30 min. Sections were then stained with primary antibody for 1 hour at room temperature and then with streptavidin–horseradish peroxidase (Jackson Immunoresearch) for 30 min followed by treatment with the TSA Bioin System tyramide staining kit (Perkin Elmer) according to the manufacturer's instructions. Sections were then stained with remaining secondary antibodies for 1 hour at room temperature. Slides were mounted with Fluoromount-G (Southern Biotech), and images were taken with a Leica SP5 inverted microscope with 40x and 63x oil immersion objectives. Images were analyzed and processed with the Imaris software and the statistics reported are average values with variability represented as standard error of the mean (SEM).

## Antibodies, Immunofluorescence and Flow Cytometry

For immunofluorescence, sections were stained with primary antibodies: Rabbit anti-GFP (A11122, Life Technologies), biotin-conjugated anti-CD35 (8C12, BD Pharmingen), goat anti-mouse IgD (goat polyclonal GAM/IGD(FC)/7S, Cedarlane Labs), APC-conjugated anti-TCRβ (457-597, eBioscience), Alexa647-conjugated anti-Bcl6 (K112-91, BD Pharmingen), biotin-conjugated anti-gp38 (8.1.1, Biolegend), APC-conjugated anti-CD21/35 (7E9, Biolegend), rat anti-mouse CD16/32 (FcγRII/III; UCSF Hybridoma Core), biotin-conjugated anti-FDC-M2 (RmC16D2, Cedarlane Labs), rat anti-mouse FDC-M1 (551320, BD Pharmigen), rabbit anti-PDGFRβ (28E1, Cell Signaling, gift from J. Rock), rabbit anti-laminin (L9393, Sigma), rat anti-VCAM1 (553330, BD Pharmingen), rabbit anti-collagen IV (ab19808, AbCam) and Alexa488 conjugated anti-GFP (A21311, Life Technologies, gift from A. Gerard). Sections were then stained with the following secondary antibodies: Alexa488-conjugated donkey anti-rabbit (A-21206, Life Technologies), Alexa555-conjugated streptavidin (S-21381, Life Technologies), AMCA-conjugated donkey anti-goat (705-156-147, Jackson Immunoresearch), biotin-conjugated donkey anti-rat (712-065-153, Jackson Immunoresearch) and Alexa647-conjugated donkey anti-rabbit (711-606-152, Jackson Immunoresearch).

For flow cytometry, single cell suspensions were generated and stained as previously described (26). The following antibodies were used for cell staining: APC-Cy7-conjugated CD45R/B220 (RA3-6B2, Biolegend), PerCp-Cy5.5-conjugated anti-IgD (11–26c.2a, Biolegend), Alexa647-conjugated anti-T- and B-Cell Activation Antigen (GL7, Biolegend) and PE-Cy7-conjugated Fas (Jo2, BD Biosciences/Fisher). Samples were acquired and analyzed with a BD LSR II and Flowjo (Treestar).

### Two-photon laser-scanning microscopy

Explant pLNs, MLNs and PPs were prepared for TPLSM as previously described for explant pLN (26) except that PP were mounted with the serosal side face-up. PPs were stabilized in a customized plastic coverslip window with Vetbond tissue glue (3M) to counter the peristaltic motion of the small intestine. The temperature at the PP during and at the end of several imaging sessions was measured using a dual-temperature controller (TC-344B, Warner Instruments) equipped with a CC-28 cable containing a bead terminator and was found to remain between 36–37 °C.

Images were acquired with ZEN2012-Black Edition (Carl Zeiss) using a 7MP two-photon microscope (Carl Zeiss) equipped with a Chameleon laser (Coherent). For video acquisition from MLNs and pLNs, a series of planes of 0.5μm (MLN) or 1μm (pLN and primary follicle pLN) Z-spacing spanning a depth of 190–260μm were collected. Each XY plane spans 283.40μm × 283.40μm at a resolution of 0.55μm per pixel (MLN, primary pLN) or 327.00μm × 327.00μm at a resolution of 0.64μm per pixel (pLN). Some images have been cropped in XY plane for optimal visualization. Excitation wavelength was 920nm. For video acquisition from PPs, a series of planes of 3μm Z-spacing spanning a depth of 50–100μm were collected every 15–30s. Each XY plane spans 425.10μm × 425.10μm at a resolution of 0.83μm per pixel or 212.55μm × 212.55μm at a resolution of 0.42μm per pixel. Excitation wavelength was 870nm. For all TPLSM imaging, emission filters were <452nm for second harmonic, 460–480nm for CFP, 500–550nm for GFP and 570–640nm for CMTMR. Videos were made and analyzed with Imaris 7.4.2 364 (Bitplane).

To track cells, surface seed points were created and tracked over time. Tracks were manually examined and verified. Data from cells that could be tracked for at least 10 min were used for analysis. Tracking data were analyzed in Microsoft Excel with a custom macro written in Microsoft Visual Basic for Applications as previously described (26). Movies were adjusted for tissue drift in Imaris 7.4.2 364 (Bitplane) and annotation and final compilation of videos were performed with iMovie (Apple). Video files were saved as .mov (Quicktime).

## RESULTS

### *Cxcl12*-expressing Reticular Cells (CRCs) populate the GC DZ niche with fine, irregular networks

To investigate the distinguishing features of GC DZ stroma across tissues, we infected *Cxcl12*-GFP reporter mice with LCMV-Armstrong and assessed the properties of the GFP-expressing CRCs. Using confocal microscopy, we identified extensive CRC networks in

splenic and pLN (inguinal, axillary and brachial) GC DZs located opposite the LZ CD35$^+$ FDCs (Fig. 1A, 1B). Chronic GCs in PPs and MLNs also contained CRC networks in the DZ (Fig. 1C), consistent with previous findings in PPs (15). Blood vessels running through the GC were also GFP$^+$ likely indicating blood endothelial cells (BECs) expressing *Cxcl12* (Fig. 1B) (15, 27).

Previous work (15) established that DZ CRC networks are distinguishable from FDCs and FRCs by their location and distinct morphology. Instead of the thick processes and consistent patterning of T zone FRCs, CRCs have fine, disorganized processes more similar to FDCs. However, CRC networks are far less dense than FDC networks. CRC processes are so thin and dispersed that 30μm stack confocal microscopy was required to visualize the networks. We identified surprising variability in CRC network structure when we imaged splenic and pLN GCs of mice responding to LCMV (Fig. 1D). In pLNs, the DZ CRCs formed mostly ‘open’ mesh structures (Fig. 1B, 1D) similar to those observed in influenza-induced mediastinal LN GCs (15). We define ‘open’ networks as having processes that extend into the LZ FDC network with no clear boundary and that become continuous with the FRC-like stroma at the T zone proximal edge of the GC at 3 or greater points. In the spleen, however, one fifth of the GCs contained CRCs with a ‘closed’ mesh structure (Fig. 1A, 1D). ‘Closed’ networks are bounded by a continuous perimeter of *Cxcl12*-GFP+ processes and connect to the FRC-like stroma at the T zone proximal edge of the GC at fewer than 3 points. About one fifth of GCs in both tissues contained both types of network (Fig. 1D). CRCs in MLN GCs and PP GCs formed open networks that frequently extended throughout the DZ (Fig. 1C).

Unlike the continuous FDC networks that fill the LZ, CRC networks frequently had an asymmetric distribution in the DZ. Of over 27 single 30μm Z-stack views of GCs from 3 mice, more than half of spleen GC DZs and almost one third of pLN GC DZs appeared only partially populated by CRCs (Fig. 1A, 1B). While tingible body macrophages (TBMs) are present in GCs and do displace stromal processes, these areas were much larger than the size of a TBM and they stained for BCL6$^+$ GC B cells (Fig. 1A, 1B). In the spleen, almost a tenth of the 30μm image stacks had no detectable CRC network in the GC (Fig. 1D). However, analysis of sequential sections of several splenic GCs revealed they all had CRCs in at least one view.

To further investigate the extent of DZ occupancy by CRCs without the extrapolation required by sections, we used two-photon laser-scanning microscopy (TPLSM) to image CRC networks in MLN GCs (Fig. 1E, Movie S1) and pLN GCs (Fig. S1A, Movie S2). SRBC-immunized *Cxcl12*-GFP mice were treated with phycoerythrin-immune complex (PE-IC) to label FDCs (TBMs are also strongly labeled) (25, 26). One day before analysis mice also received CFP transgenic B cells, which populated the follicle and outlined the GC. MLN GCs were frequently more proximal to the capsule than pLN GCs enabling higher resolution imaging of the DZ, which is orientated distal to the capsule in the GC. In agreement with our section data, we observed CRC networks in separate open and closed structures emerging from the outer edges of the DZ and leaving large areas of DZ unoccupied by detectable CRCs. The thicker 3D view also revealed that each distinct

network contained one or more CRC cell bodies, depending on the network size, and many of these cell bodies appeared bi-lobed.

To assess whether the CRC asymmetry in the DZ was a result of CRCs sharing the DZ niche with another stromal cell type or of CRCs having variable *Cxcl12* expression, we analyzed pLNs and spleen from UBI-GFP mice reconstituted with wild-type (WT) bone marrow (BM) and infected with LCMV. In these mice, all stromal cells express GFP. Surprisingly, we observed almost nine tenths of the pLN and splenic GC DZs had CRC-like networks throughout the DZ with no large areas of undetectable stroma (Fig. 1F, S1B). We saw similar results with SRBC immunized mice (Fig. S1C). These data suggest that while CRCs are a major DZ stromal cell type, GCs may contain additional DZ stromal cells that lack detectable *Cxcl12*-GFP expression.

Since CRCs in splenic DZs demonstrated more variability than CRCs in pLN DZs, we expanded on our previous investigation of CRCs in pLN primary follicles (15) to examine CRCs in splenic primary follicles. In unimmunized *Cxcl12*-GFP pLNs, CRC networks extended along the T zone proximal side of the follicle with similar morphology to pLN DZ CRC networks (Fig. 1G) as previously shown (15). In contrast, CRC networks in splenic primary follicles were less extensive than the networks in splenic GC DZs (Fig. 1H). Though they occasionally appeared to consist of only one cell in a single 30μm Z-stack, splenic primary CRCs still formed small open and closed networks in the T zone proximal region of the follicle. CRCs were detectable with a similar average frequency in pLN primary follicles (96.2% ± 3.8, n=2) as in LCMV-induced pLN GCs (100% ± 0, n=3) and in splenic primary follicles (87.1% ± 2.0, n=3) as in splenic GCs (89.8% ± 3.3, n=3). We also assessed the 3D organization of pLN primary follicle CRCs using the TPLSM analysis as described above for intact pLN DZ CRCs (Fig. S1D, Movie S2). Based on their shared *Cxcl12* expression, morphology and location, our current work and previous data (15) support the conclusion that both pLN and splenic GC CRCs arise from primary follicle CRCs.

## Movement dynamics of GC B cells in association with DZ CRCs

We next investigated whether cell-cell interactions might be important to CRC support of GC B cells in the DZ by determining if GC B cells interact with CRC processes as they move through the DZ. We attempted to visualize the interaction using TPLSM on explanted pLNs (28), but the DZ in LN GCs is orientated distal to the capsule and the fine CRC processes were too deep in the tissue to be imaged using laser intensities that preserved cell viability. In PPs, GCs form with the DZ proximal to the serosal surface and with the LZ embedded deeper in the tissue facing the subepithelial dome (29). To take advantage of this superficial positioning of the DZ, we developed an approach to label a fraction of the B cells within PP GCs. We found that when a mixture of 20% CFP transgenic B cells and 80% WT B cells was transferred into hen egg lysozyme-specific (MD4) Ig-transgenic mice for two weeks, the host GCs became dominated by the transferred B cells and about 6% of the GC B cells were $CFP^+$ (Fig. 2A). To visualize CRC-GC B cell interactions, we transferred this mixture of CFP transgenic and WT B cells into *Cxcl12*-GFP MD4 mice and, one day before imaging, injected additional CMTMR-labeled WT B cells to label a portion of the follicular

B (FOB) cells and outline the GC (Fig. 2B, Movie S3). $CFP^+$ GC B cells were observed crawling in and out of the visible DZ CRC networks, sometimes in contact with multiple processes at once, and were seen displacing the fine CRC processes as they moved (Fig. 2C, Movie S4, Movie S5). Rotation of the images showing the 3D networks revealed that the GC B cells were often completely surrounded by CRC processes (Movie S3). GC B cells in CRC networks moved with an average median velocity of 5.44μm/min ± 0.56 (n=5) and an average median turning angle of 68.04° ± 2.06 (n=5). The average median velocity was in the range described for GC B cells in pLN GCs and the average median turning angle was at the high-end of the previously described range (26, 28).

## CRCs are phenotypically distinct from FDC and FRC across tissues, but likely lineage related

Since the properties and origin of FDCs in the LZ vary between secondary lymphoid tissues (12, 30, 31), we investigated whether splenic DZ CRCs had a different relationship to FDCs and FRCs than did pLN DZ CRCs. Expanding on the initial characterization of flu-infected mediastinal LN CRCs (15), we stained lymphoid tissues from LCMV-infected and SRBC-immunized *Cxcl12*-GFP mice for canonical markers of FDCs. In splenic GCs, CRCs expressed low to undetectable levels of CD21/35 and VCAM1 (Fig. 1A, 3A) and undetectable levels of FDC-M2, FDC-M1 and CD16/32 (FcγRIII/II) (Fig. 3A). CRCs in pLN, MLN and PP GCs also expressed low to undetectable levels of CD21/35 and undetectable levels of CD16/32 (Fig. 1B, 1C, S2A) as supported by our previous work (15). PDGFRβ is widely expressed by FRCs, pericytes and other mesenchymal cells (10, 31), but this marker was undetectable on CRCs in splenic and pLN GCs as well as pLN primary follicles (Fig. 3B). Also unlike FRCs, CRCs in splenic GCs had minimal association with the reticulum, stained for with anti-laminin (Fig. 3C) and anti-type IV collagen (Fig. S2B), except at the T zone proximal edge of the GC where the CRC network meets the FRC network. This is consistent with findings in mediastinal LN GCs (15).

DZ CRCs in pLN GCs did express gp38 (podoplanin), a defining marker of FRCs, as did LZ FDCs (Fig. 3D, S2C) (32). Interestingly, we also observed $gp38^+$ stromal processes in the pLN GC DZ that were undetectable for *Cxcl12*-GFP and low to undetectable for CD35 (Fig. 3D, S2C). This is consistent with the data in Fig. 1F, S1B and S1C suggesting the presence of an additional stromal cell type in the DZ. By comparing the areas occupied by $gp38^+$ $CD35^-$ *Cxcl12*-$GFP^+$ CRC processes and $gp38^+$ $CD35^-$ *Cxcl12*-$GFP^-$ CRC processes in each of several GC DZs, we found non-CRC DZ stroma accounted for half of the DZ stromal network (50.06% ± 26.56, n=7). However, this proportion varied widely between individual GCs.

While we found CRCs to be phenotypically distinct from FDCs and FRCs, we inquired whether they might still share a precursor with these cells. To test for a relationship with FDCs, *CD21*-Cre mice (21) were crossed with *R26*-ZsGreen reporter mice. Analysis of the resulting mice revealed $CD21/35^{lo/-}$ $ZsGreen^+$ CRC-like stromal cells in spleen, MLN and pLN GC DZs and pLN primary follicles along with the expected $CD21/35^{hi}$ $ZsGreen^+$ FDCs in these tissues (Fig. 4A). We also observed the recently reported $CD21/35^-$ $ZsGreen^+$ 'versatile stromal cells' (VSCs) in the T zone in pLNs (33) and similar $CD21/35^-$ $ZsGreen^+$

FRC-like cells, possibly also VSCs, in the GC-proximal T zone in spleen and MLN (Fig. 4A). To mark *Ccl19*-expressing FRC and lineage-related cells, we crossed *Ccl19*-Cre mice (8) to *R26*-EYFP reporter mice. We found CD21/35$^{lo/-}$ EYFP$^{+}$ CRC-like stromal cells in spleen, pLN, MLN and PP GC DZs of *Ccl19*-Cre *R26*-EYFP mice along with the expected EYFP$^{+}$ T zone FRCs (Fig. 4B) (8). The majority of CD35$^{hi}$ FDCs in splenic, pLN and MLN LZs were also *Ccl19*-Cre lineage marked in agreement with previous work (8, 34). However, in PPs the extent of lineage marking of FDCs was variable (Fig. 4B). With both reporters, stroma throughout the GC DZ was lineage-marked providing strong support for the conclusion that DZ CRCs were labeled as well as any non-CRC DZ stroma. In summary, CRCs do not express most of the distinguishing markers of FDCs or FRCs, but may share a lineage precursor with both stromal cell types.

## CRCs do not require LT or TNF for maintenance of *Cxcl12* expression or network morphology

FDCs require LT and TNF signaling for their maintenance (4–6). To study whether CRCs similarly required intact LT or TNF signaling, we immunized *Cxcl12*-GFP mice with SRBCs and, on day 10, treated them with LTβR-Fc and TNFR-Fc to block signaling from the respective receptors. Four days post-treatment we observed CRC networks still visible in, and predominantly confined to, the T zone proximal side of GCs in spleen, MLN and PP (Fig. 5A, 5B). FDCs, however, no longer expressed CD35 indicating the initial decline of this population as expected with effective blockade (Fig. 5A, 5B)(5). CRC networks retained morphologies similar to those in the saline treated mice, though some splenic GCs additionally contained GFP$^{+}$ stromal cells in the T zone distal region of the GC (Fig 5A) and CRC networks in PPs receded slightly towards the serosal surface as a proportion of the GC diameter (Fig. 5A). FDCs in MLN GCs were less affected at this time-point. Therefore, across the tissues, we only quantified CRC presence in GCs with complete loss of CD35 expression on FDCs (Fig. 5B).

To better relate the observed CRC independence from LT and TNF signaling to the well-reported FDC requirement, we attempted to test whether FDCs are lost from the LZ after this short blockade or have just lost expression of essential surface markers. With the same treatment as before, we analyzed the GC stroma in UBI-GFP mice previously reconstituted with WT BM as FDCs would still be detectably GFP$^{+}$ in these mice even if they lost CD35 expression. Four days post-treatment, stromal cells were still present throughout the GC in spleen, MLN and PP (Fig. 5C, S3) suggesting FDCs were not completely lost. However, the T zone distal GC stroma no longer had the dense, mesh structure of LZ FDCs and instead consisted of dispersed processes with a morphology similar to CRCs (Fig. 5C, S3). We propose that these dispersed networks are former FDCs that have lost CD35 expression and adopted a CRC-like morphology in the absence of LT and TNF signaling. Despite the morphological similarity, we suggest these cells are not expanded CRCs based on our observation that CRCs in LTβR-Fc and TNFR-Fc treated *Cxcl12*-GFP tissues did not expand into the LZ. Thus, in a timeframe when FDCs rely on LT and TNF signaling for functional and structural maintenance, CRCs do not require LT and TNF signaling to maintain *Cxcl12* expression and network morphology.

### CXCR4 blockade disrupts CRC distribution in the GC DZ

Since GC B cells must upregulate CXCR4 to travel to the CXCL12-rich DZ (13), we investigated whether CXCR4 signaling plays a role in CRC network maintenance. Blockade of CXCR4 with genetic knockout mice or inhibitors causes GC depolarization marked by appearance of FDCs throughout the GC instead of predominantly in the LZ (13). We hypothesized that the depolarization of FDCs indicated that either CRCs were converting into FDCs or CRCs were being displaced from the DZ in absence of CXCR4 signaling. To investigate these possibilities, we treated SRBC-immunized *Cxcl12*-GFP mice with the CXCR4 inhibitor 4F-benzoyl-TE14011 or saline for 12 hours via osmotic pumps. Since the half-life of GFP *in vivo* has been estimated to be 26 hours or longer (35), this time point allowed us to assess the conversion of CRCs to FDCs even if the CRCs no longer expressed *Cxcl12*. As expected with an effective CXCR4 blockade, $CD35^+$ FDCs were detectable throughout GCs in spleen and PPs (Fig. 6). However, the dispersed stroma did not include *Cxcl12*-$GFP^+$ stroma expressing FDC markers as would have been expected if CRCs were converting to FDCs. Instead, *Cxcl12*-$GFP^+$ CRC networks were found collapsed against the DZ boundary with the T zone in splenic GCs or against the serosal-proximal lymphatics in PP GCs. Collapse of CRC networks was not observed in the GCs of saline treated mice (Fig. 6). We suggest that CRCs require CXCR4 signaling, likely in GC B cells, for structural maintenance, but not for sustaining phenotypic distinction from FDCs.

## DISCUSSION

The above findings build from recent work (15) to establish the morphology, distribution, lineage and maintenance requirements of CRCs in splenic, pLN, MLN and PP GC DZs. Our observations that DZ CRCs have low network density and variable morphology are in accord with ultrastructural studies of human tonsil GC stroma which described ‘FDCs’ in the DZ as half as dense as FDCs in the LZ and lacking in the LZ FDC ‘labyrinth-like structure’ (16, 17). Despite structural differences between CRCs and FDCs, we show GC B cells crawl in and around CRC networks with a motion similar to their activity in FDC networks (12, 26). These data suggest CRCs could likewise support GC B cells in the DZ niche through structural maintenance of the compartment and direct cell-cell interactions.

While previous studies of human tonsil GCs proposed that DZ stromal cells were a less differentiated form of LZ FDCs (16, 17), we find that CRCs and FDCs are already established as distinct populations in both pLN (15) and splenic primary follicles prior to GC formation. The role of CRCs in primary follicles is not yet clear. While naïve B cells have been shown to respond to CXCL12 for entry into pLN and entry and exit from PP (36, 37), further study is needed to characterize the effect of CRC-derived CXCL12 on naïve B cell dynamics in the primary follicle and during GC formation.

Our findings in this and previous work (15) that DZ CRCs share almost no canonical surface markers with LZ FDCs or FRCs distinguishes CRCs as a distinct cell type across different lymphoid tissues. Lacking these FDC mediators of antigen capture and integrin interaction with GC B cells (38), DZ CRCs likely make distinct contributions to the GC that meet the specialized requirements for the DZ niche (1–3). In human tonsil and LN, DZ stromal cells have similarly been reported to not express FDC markers, but have been found to express

members of the S100a family of intracellular calcium binding proteins (39–41). Future studies will be needed to discern whether murine CRCs express S100a family members uniquely among lymphoid stroma and if they contribute to CRC function in the GC.

We did find that DZ CRCs express the FRC-associated surface glycoprotein, gp38. Recently, gp38 has been described as playing a role in regulating the contraction of the LN FRC network and, as a result, the expansion of the LN after immunization (42, 43). Whether gp38 has a similar role in regulating FDC and CRC network expansion during GC formation will require future study. Additionally, our combined phenotypic characterization of CRCs as *Cxcl12*-GFP$^{+}$ gp38$^{+}$ CD31$^{-}$ PDGFRβ$^{-}$ from this and previous work (15) suggests a strategy for flow cytometric separation of CRCs from the other known *Cxcl12*-GFP$^{+}$ lymphoid stroma. This will likely be useful for investigating CRC-specific expression patterns and functions in the future.

CRCs are likely not the only stromal cells in the GC DZ. We observed that CRCs often only partially occupy GC DZs, that ubiquitous labeling of stroma shows more extensive DZ networks and that gp38$^{+}$ CD35$^{-}$ *Cxcl12*-GFP$^{-}$ reticular networks are visible in pLN DZs. These data support either the presence of an additional stromal cell type or variable *Cxcl12* expression by CRCs. GC stromal heterogeneity has precedent in an ultrastructural study of human tonsil that described 3 morphological types of DZ ‘FDCs’ and 4 morphological types of LZ ‘FDCs’ (16). Future study of the prevalence and properties of *Cxcl12*-GFP$^{-}$ DZ stroma will be needed to fully understand their relationship to CRCs and their role in the GC response.

Our lineage tracing experiments conservatively suggest that DZ stromal cells, with morphology, location and surface marker expression similar to CRCs, share a lineage relationship with FDCs, VSCs and FRCs (33). Recent studies have provided evidence that splenic FDCs develop from perivascular cells (31) whereas LN FDCs develop from marginal reticular cells (MRCs) in the outer region of the follicle (30). These cell types may similarly function as precursors for CRCs. Previous studies have shown that FDCs and FRCs are both marked by the *Ccl19*-Cre lineage reporter in pLN GCs (8, 34). Our findings suggest that DZ CRC-like stroma share this lineage across tissues. The likely common progenitor for these lymphoid stromal cells is the *Ccl19*-expressing lymphoid tissue organizer (LTo) that functions early in LN development (44). However, our finding of heterogeneity in PP FDC labeling may indicate an additional progenitor cell of distinct lineage for this population.

Our finding that DZ CRCs do not require LT and TNF signaling for short-term maintenance of *Cxcl12* expression or network morphology further distinguishes them from LZ FDCs that require these factors for their maturation and maintenance (4–6). Previous work supports the independence of *Cxcl12*-expressing stromal cells from LT and TNF signaling as *Cxcl12* expression was unaffected in spleens of LT and TNF deficient mice while *Cxcl13* expression was significantly diminished (4). These data do not exclude that DZ CRCs could depend on LT and TNF signaling for other functions.

We demonstrate that DZ CRCs depend on CXCR4, likely in GC B cells, for network distribution. We propose that the collapse of CRC networks after CXCR4 inhibition is due to GC B cells losing attraction to the CXCL12-rich DZ and collecting in the LZ, thus removing structural support from the CRC networks. The substantial hourly exchange of cells between DZ and LZ under normal conditions (45, 46) supports the possibility that the majority of DZ B cells could relocate to the LZ during the 12-hour inhibition. While DZ CRCs do not acquire an FDC phenotype with CXCR4 inhibition, CRC functions may still be impacted. While it was not possible to investigate the impact of inhibition on non-CRC DZ stroma, the complete occupancy of the GC by FDCs suggests expansion of non-CRC DZ stroma is unlikely to be the cause of CRC collapse.

Production of CXCL12 is likely one of the essential functions of CRCs in the GC DZ. However, most other secondary lymphoid stromal cells, including FRCs, BECs, lymphatic endothelial cells and red pulp fibroblasts, express *Cxcl12* outside the GC (15). Within secondary lymphoid organs, CXCL12 has established roles in promoting B and T cell entry to LNs and PPs (36), in supporting DC entry to spleen (47), in regulating egress from PPs and retention in LNs (37, 48), in aiding vascular development (49) and in guiding plasma cells to the splenic red pulp or LN medulla (50). The requirement for different stromal cell sources of CXCL12 in adjacent niches suggest there is tight control over chemokine protein distribution to create the appropriate gradients. For example, in this and previous work (15), we observed *Cxcl12* expression on blood vessels traversing both the LZ and DZ that did not seem to affect GC polarity. This is possibly due to vascular endothelial cells expressing CXCR7, a sink receptor for CXCL12 (51). How CRCs maintain the CXCL12 gradient in the DZ when *Cxcl12* is being expressed in all bordering niches remains an important question for future investigation.

## Supplementary Material

Refer to Web version on PubMed Central for supplementary material.

## Acknowledgments

We thank Y. Xu and J. An for technical assistance, A. Reboldi and H. Chen for help with TPLSM and confocal microscopy, A. Reboldi for helpful discussion, M. Matloubian for the LCMV-Armstrong, T. Nagasawa for the *Cxcl12*-GFP mice, C. Lowell for the *Ccl19*-Cre mice, L. Lanier for the *R26*-EYFP mice, K. Rajewsky for the *CD21*-Cre mice, A. Lechner and J. Rock for the PDGFRβ antibody, A. Mujal and A. Gerard for the Alexa488 conjugated anti-GFP antibody and J. Browning for LTβR-Fc and TNFR-Fc.

## References

1. Cyster JG, Ansel KM, Reif K, Ekland EH, Hyman PL, Tang HL, Luther SA, Ngo VN. Follicular stromal cells and lymphocyte homing to follicles. Immunological Reviews. 2000; 176:181–193. [PubMed: 11043777]
2. Allen CDC, Cyster JG. Follicular dendritic cell networks of primary follicles and germinal centers: phenotype and function. Seminars in Immunology. 2008; 20:14–25. [PubMed: 18261920]
3. El Shikh MEM, Pitzalis C. Follicular dendritic cells in health and disease. Front Immun. 2012; 3:292.
4. Ngo VN, Korner H, Gunn MD, Schmidt KN, Riminton DS, Cooper MD, Browning JL, Sedgwick JD, Cyster JG. Lymphotoxin alpha/beta and tumor necrosis factor are required for stromal cell

expression of homing chemokines in B and T cell areas of the spleen. J Exp Med. 1999; 189:403–412. [PubMed: 9892622]

5. Fu YX, Chaplin DD. Development and maturation of secondary lymphoid tissues. Annu Rev Immunol. 1999; 17:399–433. [PubMed: 10358764]
6. Lu TT, Browning JL. Role of the Lymphotoxin/LIGHT System in the Development and Maintenance of Reticular Networks and Vasculature in Lymphoid Tissues. Front Immun. 2014; 5:47.
7. Luther SA, Tang HL, Hyman PL, Farr AG, Cyster JG. Coexpression of the chemokines ELC and SLC by T zone stromal cells and deletion of the ELC gene in the plt/plt mouse. Proc Natl Acad Sci USA. 2000; 97:12694–12699. [PubMed: 11070085]
8. Chai Q, Onder L, Scandella E, Gil-Cruz C, Perez-Shibayama C, Cupovic J, Danuser R, Sparwasser T, Luther SA, Thiel V, Rülicke T, Stein JV, Hehlgans T, Ludewig B. Maturation of lymph node fibroblastic reticular cells from myofibroblastic precursors is critical for antiviral immunity. Immunity. 2013; 38:1013–1024. [PubMed: 23623380]
9. Link A, Vogt TK, Favre S, Britschgi MR, Acha-Orbea H, Hinz B, Cyster JG, Luther SA. Fibroblastic reticular cells in lymph nodes regulate the homeostasis of naive T cells. Nat Immunol. 2007; 8:1255–1265. [PubMed: 17893676]
10. Mueller SN, Germain RN. Stromal cell contributions to the homeostasis and functionality of the immune system. Nat Rev Immunol. 2009; 9:618–629. [PubMed: 19644499]
11. Allen CDC, Okada T, Cyster JG. Germinal-center organization and cellular dynamics. Immunity. 2007; 27:190–202. [PubMed: 17723214]
12. Wang X, Cho B, Suzuki K, Xu Y, Green JA, An J, Cyster JG. Follicular dendritic cells help establish follicle identity and promote B cell retention in germinal centers. Journal of Experimental Medicine. 2011; 208:2497–2510. [PubMed: 22042977]
13. Allen CDC, Ansel KM, Low C, Lesley R, Tamamura H, Fujii N, Cyster JG. Germinal center dark and light zone organization is mediated by CXCR4 and CXCR5. Nat Immunol. 2004; 5:943–952. [PubMed: 15300245]
14. Victora GD, Nussenzweig MC. Germinal centers. Annu Rev Immunol. 2012; 30:429–457. [PubMed: 22224772]
15. Bannard O, Horton RM, Allen CDC, An J, Nagasawa T, Cyster JG. Germinal center centroblasts transition to a centrocyte phenotype according to a timed program and depend on the dark zone for effective selection. Immunity. 2013; 39:912–924. [PubMed: 24184055]
16. Rademakers LH. Dark and light zones of germinal centres of the human tonsil: an ultrastructural study with emphasis on heterogeneity of follicular dendritic cells. Cell Tissue Res. 1992; 269:359–368. [PubMed: 1423503]
17. Imai Y, Yamakawa M. Morphology, function and pathology of follicular dendritic cells. Pathology International. 1996:807–833. [PubMed: 8970191]
18. Lefevre EA, Hein WR, Stamataki Z, Brackenbury LS, Supple EA, Hunt LG, Monaghan P, Borhis G, Richard Y, Charleston B. Fibrinogen is localized on dark zone follicular dendritic cells in vivo and enhances the proliferation and survival of a centroblastic cell line in vitro. Journal of Leukocyte Biology. 2007; 82:666–677. [PubMed: 17550975]
19. Ara T, Tokoyoda K, Sugiyama T, Egawa T, Kawabata K, Nagasawa T. Long-term hematopoietic stem cells require stromal cell-derived factor-1 for colonizing bone marrow during ontogeny. Immunity. 2003; 19:257–267. [PubMed: 12932359]
20. Schaefer BC, Schaefer ML, Kappler JW, Marrack P, Kedl RM. Observation of Antigen-Dependent CD8+ T-Cell/Dendritic Cell Interactions in Vivo. Cellular Immunology. 2001:110–122. [PubMed: 12088410]
21. Kraus M, Alimzhanov MB, Rajewsky N, Rajewsky K. Survival of resting mature B lymphocytes depends on BCR signaling via the Igalpha/beta heterodimer. Cell. 2004; 117:787–800. [PubMed: 15186779]
22. Srinivas S, Watanabe T, Lin CS, William CM, Tanabe Y, Jessell TM, Costantini F. Cre reporter strains produced by targeted insertion of EYFP and ECFP into the ROSA26 locus. BMC Dev Biol. 2001; 1:4. [PubMed: 11299042]

23. Clingan JM, Matloubian M. B Cell-intrinsic TLR7 signaling is required for optimal B cell responses during chronic viral infection. The Journal of Immunology. 2013; 191:810–818. [PubMed: 23761632]
24. Tamamura H, Hiramatsu K, Mizumoto M, Ueda S, Kusano S, Terakubo S, Akamatsu M, Yamamoto N, Trent JO, Wang Z, Peiper SC, Nakashima H, Otaka A, Fujii N. Enhancement of the T140-based pharmacophores leads to the development of more potent and bio-stable CXCR4 antagonists. Org Biomol Chem. 2003; 1:3663–3669. [PubMed: 14649897]
25. Phan TG, Grigorova I, Okada T, Cyster JG. Subcapsular encounter and complement-dependent transport of immune complexes by lymph node B cells. Nat Immunol. 2007; 8:992–1000. [PubMed: 17660822]
26. Allen CDC, Okada T, Tang HL, Cyster JG. Imaging of germinal center selection events during affinity maturation. Science. 2007; 315:528–531. [PubMed: 17185562]
27. Ding L, Morrison SJ. Haematopoietic stem cells and early lymphoid progenitors occupy distinct bone marrow niches. Nature. 2013; 495:231–235. [PubMed: 23434755]
28. Suzuki K, Grigorova I, Phan TG, Kelly LM, Cyster JG. Visualizing B cell capture of cognate antigen from follicular dendritic cells. Journal of Experimental Medicine. 2009; 206:1485–1493. [PubMed: 19506051]
29. Lelouard H, Fallet M, de Bovis B, Méresse S, Gorvel JP. Peyer's patch dendritic cells sample antigens by extending dendrites through M cell-specific transcellular pores. Gastroenterology. 2012; 142:592–601. [PubMed: 22155637]
30. Jarjour M, Jorquera A, Mondor I, Wienert S, Narang P, Coles MC, Klauschen F, Bajénoff M. Fate mapping reveals origin and dynamics of lymph node follicular dendritic cells. Journal of Experimental Medicine. 2014; 211:1109–1122. [PubMed: 24863064]
31. Krautler NJ, Kana V, Kranich J, Tian Y, Perera D, Lemm D, Schwarz P, Armulik A, Browning JL, Tallquist M, Buch T, Oliveira-Martins JB, Zhu C, Hermann M, Wagner U, Brink R, Heikenwalder M, Aguzzi A. Follicular Dendritic Cells Emerge from Ubiquitous Perivascular Precursors. Cell. 2012; 150:194–206. [PubMed: 22770220]
32. Mueller SN, Hosiawa-Meagher KA, Konieczny BT, Sullivan BM, Bachmann MF, Locksley RM, Ahmed R, Matloubian M. Regulation of Homeostatic Chemokine Expression and Cell Trafficking During Immune Responses. Science. 2007; 317:670–674. [PubMed: 17673664]
33. Mionnet C, Mondor I, Jorquera A, Loosveld M, Maurizio J, Arcangeli M-L, Ruddle NH, Nowak J, Aurrand-Lions M, Luche H, Bajénoff M. Identification of a new stromal cell type involved in the regulation of inflamed B cell follicles. PLoS Biol. 2013; 11:e1001672. [PubMed: 24130458]
34. Fasnacht N, Huang HY, Koch U, Favre S, Auderset F, Chai Q, Onder L, Kallert S, Pinschewer DD, MacDonald HR, Tacchini-Cottier F, Ludewig B, Luther SA, Radtke F. Specific fibroblastic niches in secondary lymphoid organs orchestrate distinct Notch-regulated immune responses. Journal of Experimental Medicine. 2014; 211:2265–2279. [PubMed: 25311507]
35. Corish P, Tyler-Smith C. Attenuation of green fluorescent protein half-life in mammalian cells. Protein Eng. 1999; 12:1035–1040. [PubMed: 10611396]
36. Okada T V, Ngo N, Ekland EH, Förster R, Lipp M, Littman DR, Cyster JG. Chemokine requirements for B cell entry to lymph nodes and Peyer's patches. J Exp Med. 2002; 196:65–75. [PubMed: 12093871]
37. Schmidt TH, Bannard O, Gray EE, Cyster JG. CXCR4 promotes B cell egress from Peyer's patches. Journal of Experimental Medicine. 2013; 210:1099–1107. [PubMed: 23669394]
38. Wang X, Rodda LB, Bannard O, Cyster JG. Integrin-mediated interactions between B cells and follicular dendritic cells influence germinal center B cell fitness. The Journal of Immunology. 2014; 192:4601–4609. [PubMed: 24740506]
39. Tsunoda T, Yamakawa M, Takahashi T. Differential expression of Ca(2+)-binding proteins on follicular dendritic cells in non-neoplastic and neoplastic lymphoid follicles. The American Journal of Pathology. 1999; 155:805–814. [PubMed: 10487838]
40. Kasajima-Akatsuka N, Maeda K. Development, maturation and subsequent activation of follicular dendritic cells (FDC): immunohistochemical observation of human fetal and adult lymph nodes. Histochem Cell Biol. 2006; 126:261–273. [PubMed: 16470387]

41. Maeda K, Matsuda M, Suzuki H, Saitoh HA. Immunohistochemical recognition of human follicular dendritic cells (FDCs) in routinely processed paraffin sections. J Histochem Cytochem. 2002; 50:1475–1486. [PubMed: 12417613]

42. Acton SE, Farrugia AJ, Astarita JL, Mourão-Sá D, Jenkins RP, Nye E, Hooper S, van Blijswijk J, Rogers NC, Snelgrove KJ, Rosewell I, Moita LF, Stamp G, Turley SJ, Sahai E, Reis e Sousa C. Dendritic cells control fibroblastic reticular network tension and lymph node expansion. Nature. 2014; 514:498–502. [PubMed: 25341788]

43. Astarita JL, Cremasco V, Fu J, Darnell MC, Peck JR, Nieves-Bonilla JM, Song K, Kondo Y, Woodruff MC, Gogineni A, Onder L, Ludewig B, Weimer RM, Carroll MC, Mooney DJ, Xia L, Turley SJ. The CLEC-2-podoplanin axis controls the contractility of fibroblastic reticular cells and lymph node microarchitecture. Nat Immunol. 2015; 16:75–84. [PubMed: 25347465]

44. van de Pavert SA, Mebius RE. New insights into the development of lymphoid tissues. Nat Rev Immunol. 2010; 10:664–674. [PubMed: 20706277]

45. Beltman JB, Allen CDC, Cyster JG, de Boer RJ. B cells within germinal centers migrate preferentially from dark to light zone. Proceedings of the National Academy of Sciences. 2011; 108:8755–8760.

46. Victora GD, Schwickert TA, Fooksman DR, Kamphorst AO, Meyer-Hermann M, Dustin ML, Nussenzweig MC. Germinal center dynamics revealed by multiphoton microscopy with a photoactivatable fluorescent reporter. Cell. 2010; 143:592–605. [PubMed: 21074050]

47. Umemoto E, Otani K, Ikeno T, Verjan Garcia N, Hayasaka H, Bai Z, Jang MH, Tanaka T, Nagasawa T, Ueda K, Miyasaka M. Constitutive plasmacytoid dendritic cell migration to the splenic white pulp is cooperatively regulated by CCR7- and CXCR4-mediated signaling. The Journal of Immunology. 2012; 189:191–199. [PubMed: 22634622]

48. Nakai A, Hayano Y, Furuta F, Noda M, Suzuki K. Control of lymphocyte egress from lymph nodes through β2-adrenergic receptors. Journal of Experimental Medicine. 2014; 211:2583–2598. [PubMed: 25422496]

49. Griffith JW, Sokol CL, Luster AD. Chemokines and chemokine receptors: positioning cells for host defense and immunity. Annu Rev Immunol. 2014; 32:659–702. [PubMed: 24655300]

50. Hargreaves DC, Hyman PL, Lu TT, Ngo VN, Bidgol A, Suzuki G, Zou YR, Littman DR, Cyster JG. A coordinated change in chemokine responsiveness guides plasma cell movements. J Exp Med. 2001; 194:45–56. [PubMed: 11435471]

51. Sierro F, Biben C, Martínez-Muñoz L, Mellado M, Ransohoff RM, Li M, Woehl B, Leung H, Groom J, Batten M, Harvey RP, Martínez-A C, Mackay CR, Mackay F. Disrupted cardiac development but normal hematopoiesis in mice deficient in the second CXCL12/SDF-1 receptor, CXCR7. Proc Natl Acad Sci USA. 2007; 104:14759–14764. [PubMed: 17804806]

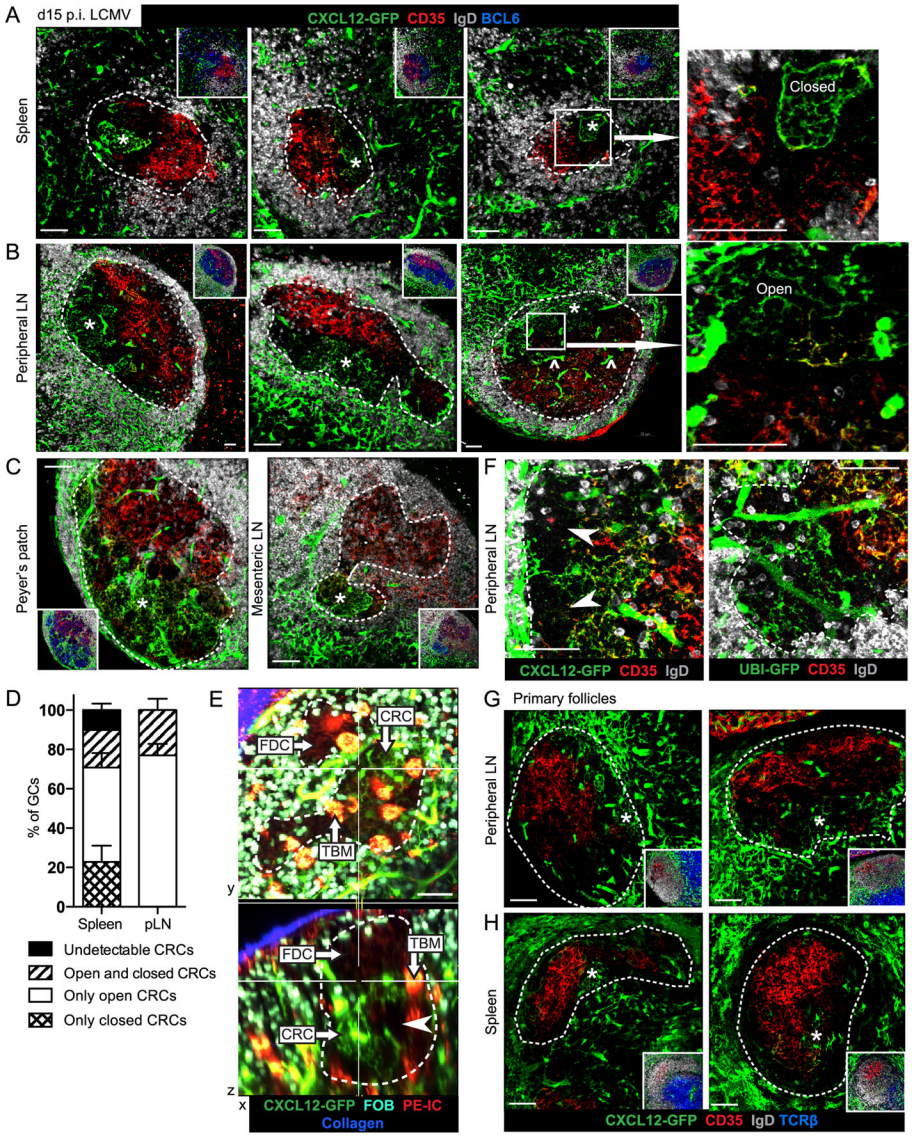


**FIGURE 1.** ***Cxcl12*-expressing Reticular Cells (CRCs) populate the DZ niche with fine, irregular networks**

**(A–C)** Thick section (30μm) confocal microscopy of *Cxcl12*-GFP$^{+}$ DZ CRCs (*) and CD35$^{+}$ FDCs in tissues from *Cxcl12*-GFP mice analyzed at day 15 post-infection (p.i) with LCMV. (^) Blood vessel passing through GC. White box and arrow indicate increased magnification of CRCs in 'closed' formation in spleen (**A**) and in 'open' formation in pLN (**B**). White, dotted line indicates the GC boundary based on BCL6 staining only shown in insets. Data (A–C) are representative of 3 mice and 3–15 GC views per tissue per mouse. **(D)** Average frequency of DZ CRC network morphologies observed in thick sections from 3 LCMV-infected mice with 6–15 GC views per tissue, error bars represent SEM. **(E)** TPLSM of intact *Cxcl12*-GFP MLN GC on day 10 post-immunization with SRBCs and 1 day after transfer of CFP$^{+}$ naïve B cells (follicular B cells, FOB) to mark the GC edge (white, dotted line) and treatment with PE-IC to label FDCs and TBMs. CRCs, FDCs and TBMs are labeled and areas of undetectable DZ stroma indicated (arrowhead) in XY and XZ sections

of the 193μm z-stack shown as maximum intensity projections (x=5.54μm, y=6.09μm, z=30.0μm). Images correspond to Movie S1. Representative of 2 mice and 4 GCs per MLN. **(F)** Regions of undetectable stroma (arrowhead) in pLN GC DZs from *Cxcl12*-GFP mice (3 mice, 3–15 GCs views per mouse) and UBI-GFP mice previously reconstituted with WT BM (2 mice, 1–7 GCs views per mouse) imaged on day 15 p.i. with LCMV. White dotted line indicates the GC boundary based on IgD stain. **(G and H)** Confocal microscopy of CRCs (*) in primary follicles from (**G)** pLN (2 mice, 6–26 follicle views per mouse) and **(H)** spleen (3 mice, 20–90 follicle views per mouse) from unimmunized *Cxcl12*-GFP mice. White, dotted line indicates the boundary of the primary follicle based on TCRβ and IgD stain only shown in insets. Scale bar is 50μm.

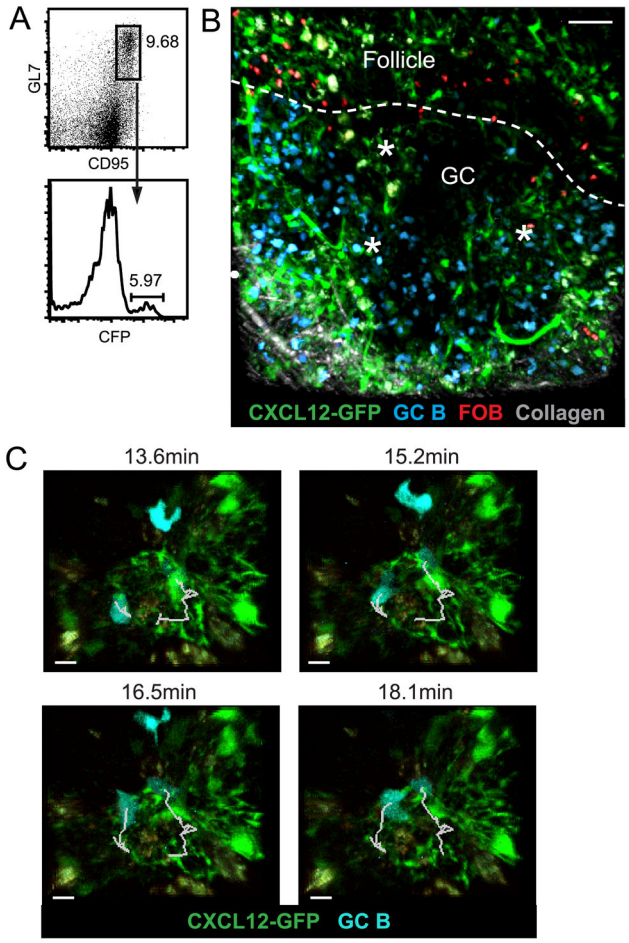


**FIGURE 2. Movement dynamics of GC B cells in association with DZ CRCs**

TPLSM of *Cxcl12*-GFP MD4 PPs 2 weeks after transfer of WT and $CFP^+$ B cells and 1 day after transfer of CMTMR-labeled WT B cells to label a portion of the FOB cells and outline the GC (white, dotted line). **(A)** Representative flow cytometry plots showing percent of $CFP^+$ GC B cells ($B220^+$ $IgD^-$ $GL7^+$ $CD95^+$) in PPs on day of imaging. Pre-gated for $B220^+$ $IgD^-$ cells, numbers indicate percent of parent gate**. (B)** CRC networks (*) in explant PP GC DZ (60μm z-stack) surrounded by $CFP^+$ GC B cells. Collagen marks the serosal edge of the PP. Images correspond to Movie S3 and S4. Scale bar is 50μm. **(C)** Time lapse images of $CFP^+$ GC B cells moving through $GFP^+$ CRC networks in an explant PP (69μm z-stack). Tracks of GC B cells indicated in white. Images correspond to Movie S5. Scale bar is 10μm. Images representative of 6 movies from 3 mice in 3 experiments.

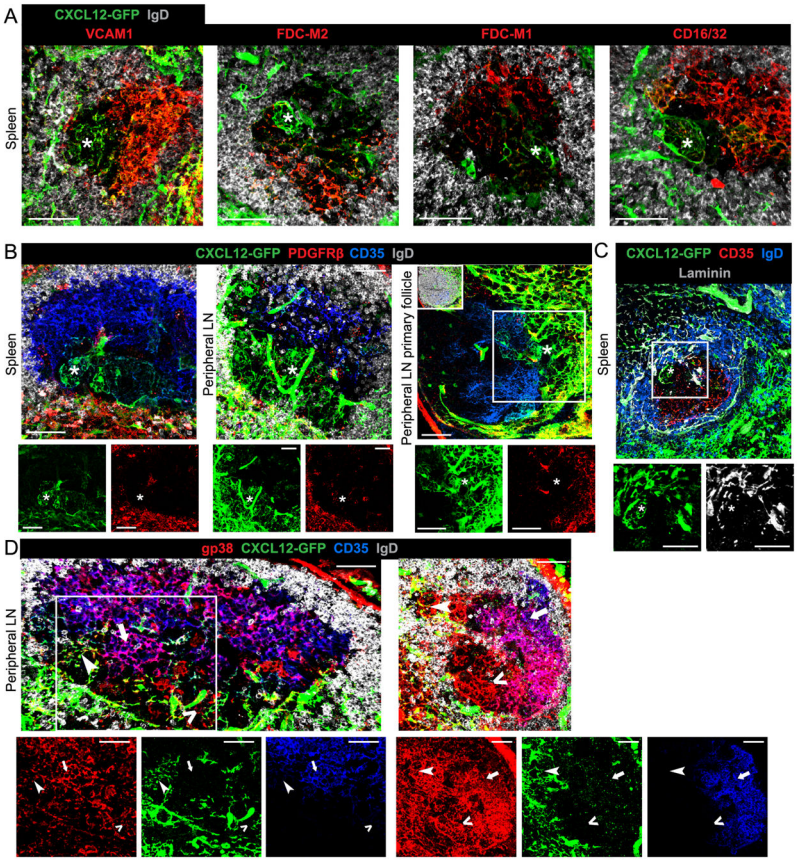


**FIGURE 3. CRCs are phenotypically distinct from FDCs and FRCs across tissues**

Confocal microscopy of CRCs (*) in GCs from SRBC-immunized *Cxcl12*-GFP mice stained for **(A)** VCAM1, FDC-M2, FDC-M1 and CD16/32 (each image representative of 1–3 mice, 2–20 GC views per spleen), **(B)** GCs and primary follicles stained for PDGFRβ (1–3 mice, 14 GC views per spleen, 2–3 GC views per pLN, 4 follicle views per pLN). In primary pLN panel, IgD is only shown in inset and white box indicates area shown in single channels. **(C)** GC stained for laminin (3 mice, 1–3 GC views per spleen). **(D)** PLN GCs from *Cxcl12*-GFP mice on day 15 p.i. with LCMV stained for gp38 (2 mice, 1–18 GC views per mouse). Examples of CRCs (arrowhead), FDCs (arrow) and gp38$^{+}$ CD35$^{-}$ *Cxcl12*-GFP$^{-}$ stroma (^) are indicated. (C and D) Individual channels shown below merged image and if enlarged, area indicated by white box. Scale bar is 50μm.

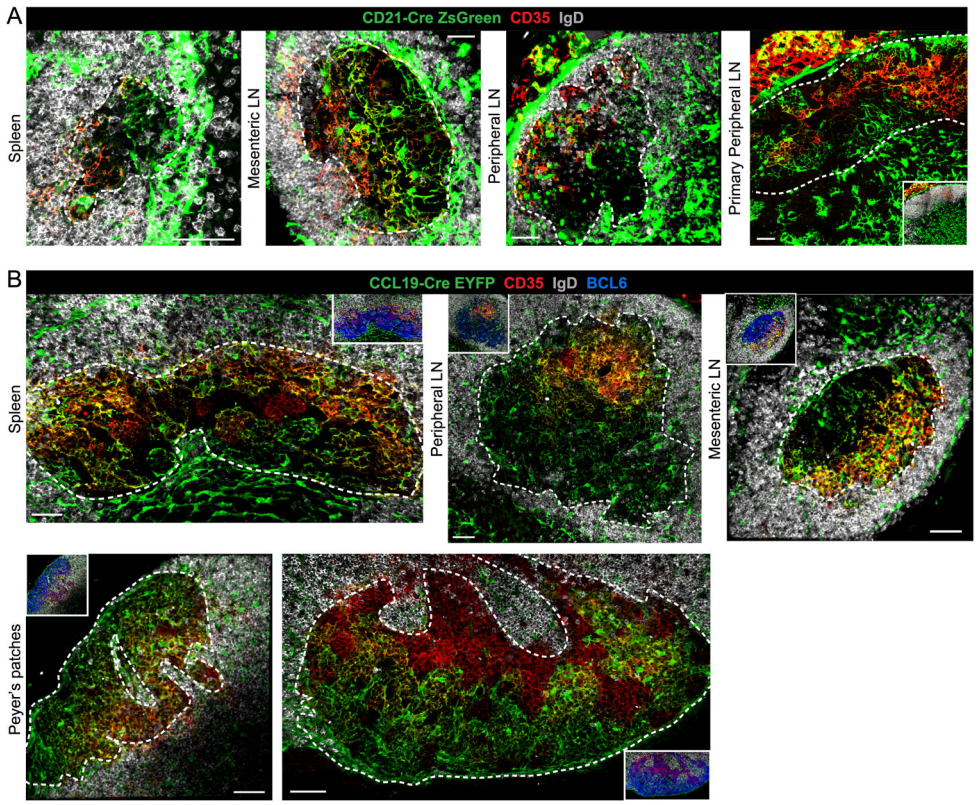


**FIGURE 4. CRCs are likely lineage related to FDCs and FRCs**

Confocal microscopy of CRCs (*) in GCs from SRBC-immunized **(A)** *CD21*-Cre *R26*-ZsGreen lineage reporter mice (1–4 mice, 3–14 GC views per spleen, 2–5 GC views per MLN, 3–10 GC views per pLN and 2 follicle views per primary pLN) and **(B)** *Ccl19*-Cre *R26*-EYFP lineage reporter mice (3 mice, 6–7 GC views per spleen, 2–6 GC views per pLN, 1–7 GC views per MLN and 1–3 GC views per PP). White, dotted line outlines GCs **(A and B)** based on $BCL6^+$ GC B cell stain (inset only) and pLN primary follicle **(A)** based on $IgD^+$ FOB cell stain (inset only). Scale bar is 50μm.

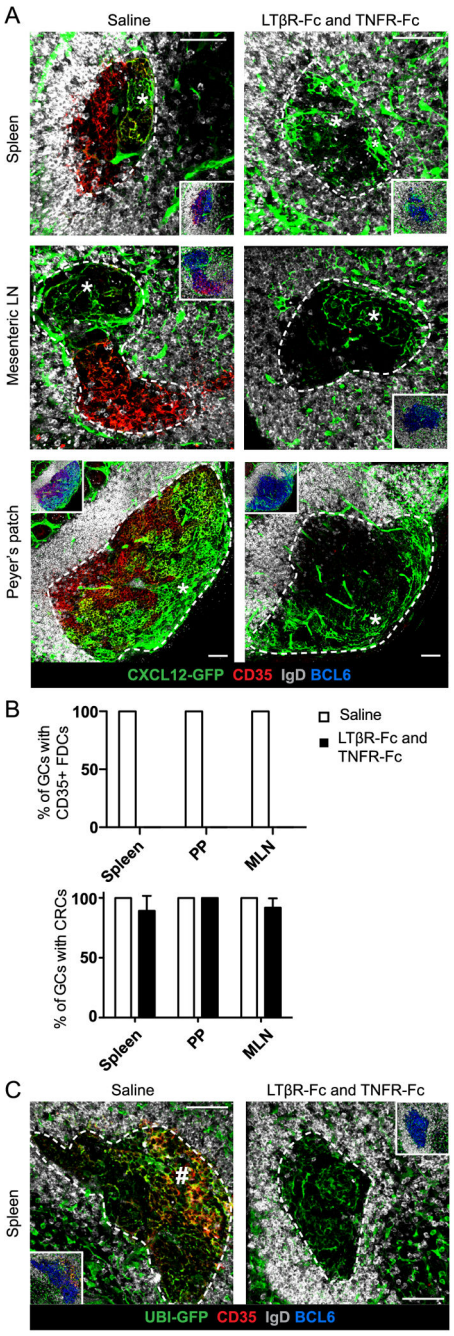


**FIGURE 5. CRCs do not require LT or TNF signaling for maintenance of *Cxcl12* expression or network morphology**

**(A)** Confocal microscopy images of GC CRC networks (*) in *Cxcl12*-GFP mice immunized with SRBC and, on day 10, treated with 1mg/ml LTβR-Fc and 1mg/ml TNFR-Fc or saline. Mice were analyzed on day 14. **(B)** Percent of GCs containing $CD35^{+}$ FDCs (top) or CRC networks (bottom). Data from 3 mice treated with saline (6–23 GC views per spleen, 5–14 GC views per MLN, 5–6 GC views per PP) and 4 mice treated with LTβR-Fc + TNFR-Fc (8–26 GC views per spleen, 2–13 GC views per MLN, 2–9 GC views per PP) represented as mean and error bars represent SEM. **(C)** Splenic GCs from UBI-GFP mice reconstituted

with WT BM and treated as in (A). Dense, mesh structure of $CD35^+$ FDCs indicated (#). Data are representative of 3 mice treated with saline (9–13 GC views per spleen) and 3 mice treated with LTβR-Fc + TNFR-Fc (10–17 GC views per spleen). **(A and C)** GCs outlined with white, dotted line based on $BCL6^+$ GC B cell stain (inset only). Scale bar is 50μm.

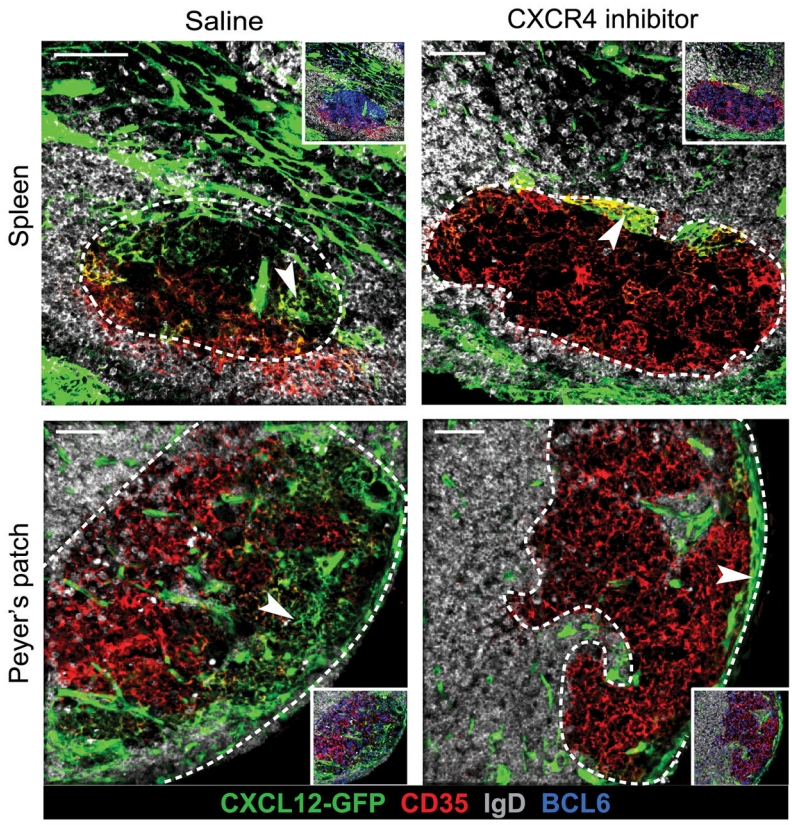


**FIGURE 6. CXCR4 blockade disrupts CRC distribution in the GC DZ**

Confocal microscopy of CRC networks (arrowheads) in splenic and PP GCs of *Cxcl12*-GFP mice after treatment with a CXCR4 inhibitor for 12 hours. GCs outlined with white, dotted line based on $BCL6^{+}$ GC B cells (inset only). Images are representative of 1 mouse treated with saline (6–39 GC views per tissue) and 1–2 mice treated with CXCR4 inhibitor (4–27 GC views per tissue). Similar results found with treatment for 24 hours (1 mouse treated with saline and 1 mouse treated with CXCR4 inhibitor). Scale bar is 50μm.